

1 **Relative contribution of atmospheric drivers to**
2 **‘extreme’ snowfall over the Amundsen Sea Embayment**

3 ¹ Sai Prabala Swetha Chittella

4 ² Pranab Deb

5 ³ Jan Melchior van Wessem

6 ^{1,2}Centre for Oceans, Rivers, Atmosphere and Land Sciences, Indian Institute of Technology Kharagpur
7 ³Institute for Marine and Atmospheric Research Utrecht, Utrecht University, Utrecht, the Netherlands

8 **Key Points:**

- 9 • The main drivers of extreme snowfall events over Amundsen Sea Embayment are
10 identified, and their relative contribution is quantified
11 • A coupled pattern consisting of Amundsen Sea low and a blocking high to the east is
12 the dominant driver of extreme snowfall during 1979-2016
13 • El Niño Southern Oscillation and ‘atmospheric rivers’ are also suspected to be linked
14 to several extreme snowfall events over the region

Corresponding author: Pranab Deb, pranab@coral.iitkgp.ac.in

Abstract

We investigate the atmospheric drivers of extreme precipitation over the Amundsen Sea Embayment (ASE) of West Antarctica using daily output from RACMO2 model and reanalysis data (1979-2016). Overall, 93.7% of days with extreme precipitation at the 2 coastal stations of ASE are associated with the 4 dominant Empirical Orthogonal Function (EOF) modes of geopotential height anomalies (at 850 hPa) over West Antarctica. The second EOF mode, associated with a coupled pattern consisting of Amundsen Sea Low and a blocking high to the east, is the main driver of extreme precipitation over ASE, linked to 44.75% of extreme precipitation days. This is followed by EOF-3 (associated with El Niño Southern Oscillation/PSA-1), EOF-4 (likely associated with more frequent ‘atmospheric river’ events) and EOF-1 (i.e., Southern Annular mode) with a contribution of 22.16%, 21.1% and 12%, respectively. Extreme precipitation linked to EOF-2 and EOF-4 are more intense (by ~ 2 mm/day) than the rest.

Plain Language Summary

Snowfall is a key component of the mass balance or ‘stability’ of the West Antarctic ice sheet. Around 35% of the total precipitation over the Amundsen Sea Embayment of West Antarctica comes from “extreme” snowfall events. We analyse the output from a regional climate model and global reanalysis data to study the seasonal distribution of these extreme events. We identify the atmospheric patterns responsible for these events, and quantify their relative importance. The low pressure system over Amundsen Sea was found to be the dominant driver of these events. Remote forcing due to periodic warming of the tropical Pacific Ocean can also lead to extreme snowfall over the region. Moreover, atmospheric patterns conducive to frequent “atmospheric rivers” events over West Antarctica can cause intense snowfall events in the region.

1 Introduction

The contribution of Antarctic Ice Sheet to the global sea level rise has increased in recent decades, primarily due to ice loss driven by basal melting of ice shelves in West Antarctica (WA) and Antarctic Peninsula (H. Pritchard et al., 2012). The accumulated contribution of WA to sea level rise is 6.9 ± 0.6 mm since 1979 (Rignot et al., 2019). Warmer ocean temperature and incursions of warm circumpolar deep water onto the continental shelf are considered to be the key processes driving the basal melting of WA ice shelves (Vaughan et al., 2001; Mayewski et al., 2009; Summerhayes et al., 2009; Turner et al., 2009).

Antarctic Mass Balance is maintained by accumulation of precipitation, blowing snow and ice loss due to melting, evaporation/sublimation and calving of ice along the coast. The accelerated mass loss from the continent (Rignot et al., 2008; H. D. Pritchard et al., 2009) is partially compensated by snowfall (Zwally et al., 2017; Paolo et al., 2018). As the atmospheric moisture content over Antarctica is low, precipitation in coastal regions is mainly dominated by intense ‘high’ precipitation events which are highly episodic, and driven by moisture transport from low-latitude areas associated with certain synoptic conditions (Noone & Simmonds, 1998; Sodemann & Stohl, 2009). Generally, these extreme precipitation events (EPEs) are responsible for most of the annual precipitation over coastal Antarctica (Turner et al., 2019). Turner et al. (2009) demonstrated that during 1979–2016, around 70% of the variance in annual precipitation of Antarctica is accounted for by variability in EPEs, with the figure rising to 97% at one location over the Amundsen Sea Embayment (ASE) (83°S , 146°W). Another recent study (Maclennan & Lenaerts, 2021) documents the importance of EPEs over the Thwaites Glacier region in WA, with EPEs accounting for around 60% of the total snowfall.

The spatial variability of different atmospheric and cryospheric parameters in WA is largely

65 controlled by the large-scale circulation patterns in the southern high latitudes, e.g., the
66 Southern Annular Mode (SAM), the Pacific-South American (PSA1 and PSA2) patterns
67 (Ghil & Mo, 1991; Lau et al., 1994; Kidson, 1988; Deb et al., 2016; G. J. Marshall et al.,
68 2017). The PSA1 pattern is known to be modulated by sea surface temperature anomalies
69 over tropical eastern Pacific Ocean i.e., ENSO variability (Mo & Paegle, 2001). ASE
70 has the strongest teleconnection to ENSO manifested via modifications in the Amundsen
71 Sea Low (ASL) (Deb et al., 2018). PSA2 is a dominant zonal wavenumber-3 pattern in
72 Southern Hemisphere which is also found to be influenced by tropical western Pacific Ocean
73 (M. Raphael, 2004; Clem & Fogt, 2015; Irving & Simmonds, 2015). A coupled atmospheric
74 structure consisting of a blocking high to the west of Antarctic Peninsula and the ASL
75 represents the western branch of the PSA2 pattern (M. Raphael, 2004), and drives a strong
76 meridional flow towards the coastal WA (Deb et al., 2018). G. J. Marshall et al. (2017)
77 showed that polarities of these principal modes of atmospheric circulation control the EPEs
78 over Antarctica. Moreover, “atmospheric rivers” that carry large quantities of moisture from
79 midlatitudes have also been linked to several coastal EPEs in Antarctica (Zhu & Newell,
80 1998; Gorodetskaya et al., 2014).

81
82 The scarcity and uneven distribution of observation records limit our understanding of the
83 fine scale distribution of precipitation, particularly over the coastal regions (Banta et al.,
84 2008; Maclennan & Lenaerts, 2021). Moreover reanalysis products and global climate model
85 simulations are too coarse to capture the complex spatial pattern of topography and related
86 meteorological processes over the region (Orr et al., 2014; Deb et al., 2016). To this end,
87 dynamical downscaling of global reanalysis data using limited-area high-resolution regional
88 atmospheric models (e.g., Giorgi et al. (1994)) has emerged as a useful tool to generate
89 physically consistent temporal and spatial pattern of Antarctic precipitation (J. T. Lenaerts
90 et al., 2013; G. J. Marshall et al., 2017). For example, the performance of the Regional
91 Atmospheric Climate Model (RACMO) has been vetted by two recent studies in capturing
92 the mean and extreme precipitation over Antarctica (Turner et al., 2019; Maclennan
93 & Lenaerts, 2021). These studies have attempted to quantify the variability and contribu-
94 tion of extreme snowfall events over Antarctica (Turner et al., 2019), and to identify the
95 atmospheric drivers of EPEs over the Thwaites glacier region of WA (e.g., Thwaites glacier).

96
97 However, no studies exist that quantify the role of dominant atmospheric drivers of EPEs
98 across the ASE, or quantify the seasonal contribution of these drivers to the occurrence of
99 EPEs. Here, we present the intensity and frequency of EPEs over ASE using output from
100 a high-resolution regional climate model (RACMO2). Thereafter, we identify the primary
101 atmospheric drivers of these EPEs, and quantify their relative and seasonal contribution.

102 2 Data and methods

103 Daily precipitation flux derived from an Antarctic-wide simulation of RACMO2 (version
104 2.3, Van Wessem et al. (2014)) during the period from 1979-2016 (January to December) is
105 used to calculate daily precipitation (mm/day). The model uses a horizontal resolution of
106 27 km and a vertical resolution of 40 levels. The model combines the atmospheric dynam-
107 ics of the High Resolution Limited Area Model (HIRLAM; Undén et al. (2002)) with the
108 physics package of the European Centre for Medium-Range Weather Forecasts (ECMWF)
109 Integrated Forecast System (IFS). The model is forced by 6-hourly ERA-Interim reanalysis
110 data (Dee et al., 2011), and the interior of domain is set free while the lateral and ocean
111 boundaries are constrained. This model version 2.3 is optimised for polar regions by inter-
112 actively coupling it to a multilayer snow model (Ettema et al., 2010). A prognostic scheme
113 for snow grain size is used for the calculation of snow albedo (Kuipers Munneke et al., 2011)
114 while the interaction of the near-surface air with drifting snow is simulated by drifting snow
115 scheme (Déry & Yau, 1999; J. Lenaerts et al., 2010).

116
117 We define daily EPEs as days during which daily precipitation exceeds the 95th percentile of

118 daily precipitation values of the whole time series. Empirical Orthogonal Function (EOF)
 119 analysis of daily geopotential height anomaly was performed to identify the dominant pat-
 120 terns of atmospheric variability over WA. Spatial patterns of the major EOF modes over
 121 the domain encompassing 60°-90°S and 180°-60°W were computed by considering the daily
 122 geopotential height anomalies at 850 hPa derived from ERA-Interim reanalysis at a hori-
 123 zontal resolution of 0.75° by 0.75° during 1979-2016. The time series of these EOF modes
 124 are called principal components (PCs), are normalised such that their mean is zero and
 125 standard deviation is one. Next, the values of the normalised major PCs are extracted for
 126 each EPE day. For a particular EPE day, a PC mode is considered to be dominant if the
 127 magnitude of the normalised PC is greater than 1 for that day.

128
 129 Further, moisture divergence and moisture transport data derived from ERA-Interim re-
 130 analysis were used to study the atmospheric condition during EPE days. To identify the
 131 climatic drivers of the EPEs, several global climate indices were also analysed, e.g., ENSO-
 132 Oceanic Niño Index (ONI)(National Weather Service, Climate Prediction Center), Marshall
 133 SAM index (G. Marshall, 2018) and ASL index (S. Hosking, 2020). We also define an ASL-
 134 lon index, following Deb et al. (2018), as the difference between mean sea level pressure
 135 averaged over a box in the western Amundsen Sea region (to the west of 125°W; labeled
 136 “Box 1” in Figure-1a) and a box in the Bellingshausen Sea (to the east of 110°W, labeled
 137 “Box 2” in Figure-1a). Positive (negative) values of index indicates the eastward (westward)
 138 shift of the location of the ASL. This index effectively captures the blocking pattern over
 139 WA and the zonal migration of ASL.

140 3 Results

141 Spatial distribution of average daily precipitation over WA during 1979-2016 is shown in
 142 Figure-1b. Coastal areas with elevation less than 1000 m are associated with higher average
 143 precipitation values (> 3 mm/day). The average precipitation values drop down to below
 144 2 mm/day in the inland areas. Over the coastal areas, the mean daily precipitation from
 145 EPEs (Figure-1c) is approximately 7 times more than that of average daily precipitation
 146 (Figure-1b). Figure-1d shows that the difference of average precipitation from EPEs and
 147 average daily precipitation is maximum in the coastal areas (~ 16 – 34 mm/day). The mean
 148 precipitation from EPEs is much lower (difference < 10 mm/day) further inland when com-
 149 pared to coastal areas. Overall, the total precipitation accumulated for the whole domain
 150 (outlined in thick red lines in Figure-1a) is 1.9471×10^4 Gt out of which the total contribution
 151 from EPEs is 6.8523×10^3 Gt during 1979-2016. Thus, EPEs contribute 35.19% to the total
 152 precipitation over the WA domain.

153
 154 In coastal areas, the mean precipitation linked to EPEs show large values, particularly
 155 over the ASE region. In order to capture the characteristics and drivers of EPEs over the
 156 ASE, two coastal locations, namely Evans Knoll (EK, red circle in Figure-1e) and Bear
 157 Peninsula (BP, magenta circle in Figure-1f), are selected. The time series of average daily
 158 precipitation from the two stations are closely related to each another (correlation of 0.7).
 159 Moreover, the daily average precipitation at these two stations are significantly correlated
 160 to a large portion of the WA, with particularly high correlation over the ASE (Figures-1e
 161 and 1f). The precipitation over EK shows the strongest correlation with precipitation over
 162 ASE to the east of 115°W (correlation > 0.6), while the precipitation over BP is strongly
 163 associated with precipitation over ASE to the west of 95°W (correlation > 0.6). Since, the
 164 precipitation at these two locations are representative of precipitation over the entire ASE
 165 (and also over a larger WA domain), we focus on these locations instead of area averaged
 166 values over ASE.

167
 168 The frequency distribution and seasonality of EPEs are similar at both the locations (Sup-
 169plementary Figure-S1 and S2). The maximum number of EPEs occurring in JJA, followed
 170 by MAM and SON and significantly less number of EPEs are found in DJF (Supplementary

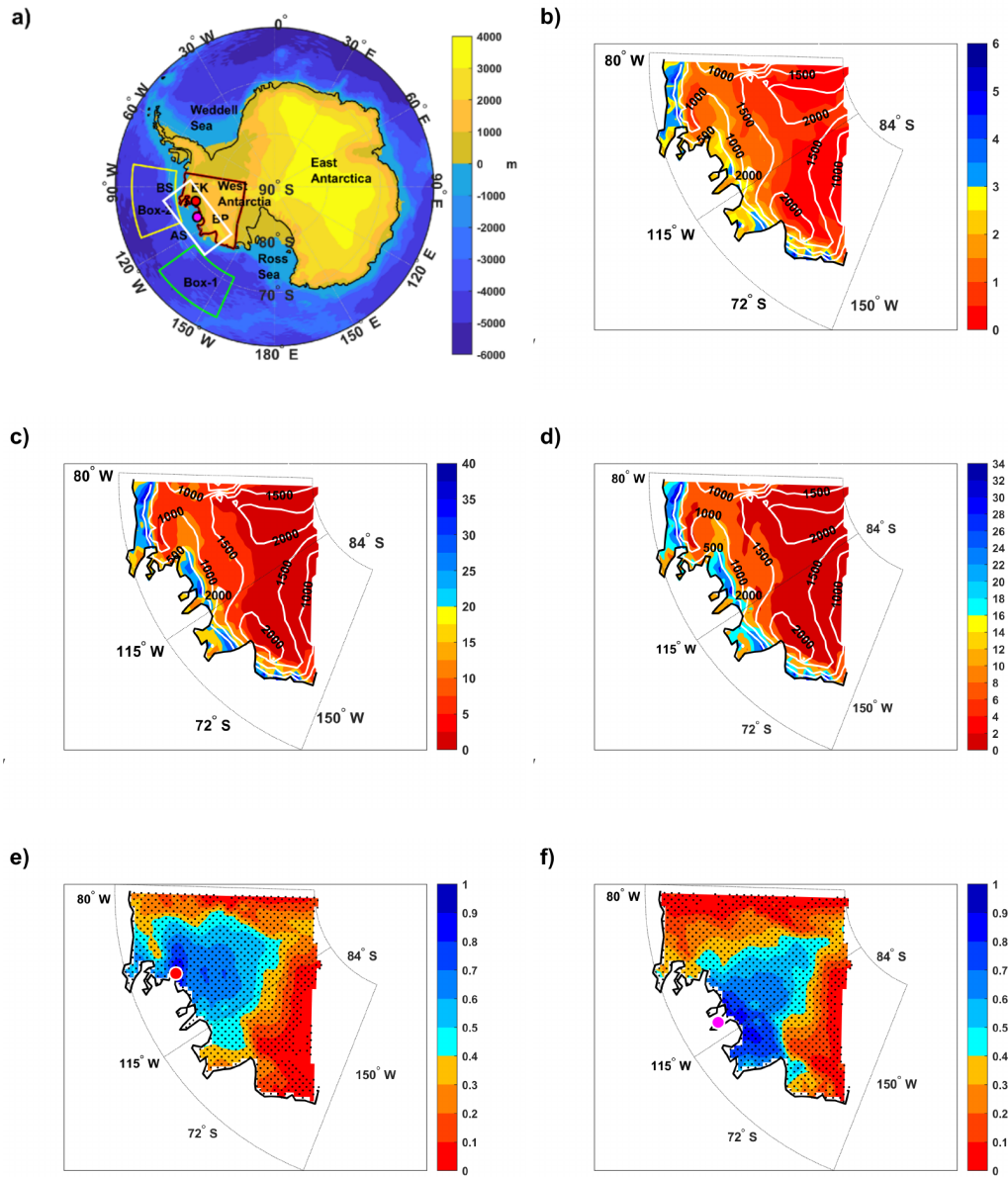


Figure 1. (a) Map of Antarctica with surface elevation in the background (shaded, in m). The Study area outlined in thick red lines. White box is the region of Amundsen Sea Embayment. EK-Evans Knoll, BP-Bear Peninsula, BS- Bellingshausen sea, AS-Amundsen sea, box-1 and box-2 are regions in AS and BS. Spatial distribution of (b) average daily precipitation (mm/day) and (c) average precipitation (mm/day) from all EPEs at each grid of study area for time period 1979-2016.(d) Difference of average precipitation from EPEs and average daily precipitation. Correlation between (e) Evans Knoll and (f) Bear Peninsula to study domain at 95% significant level.

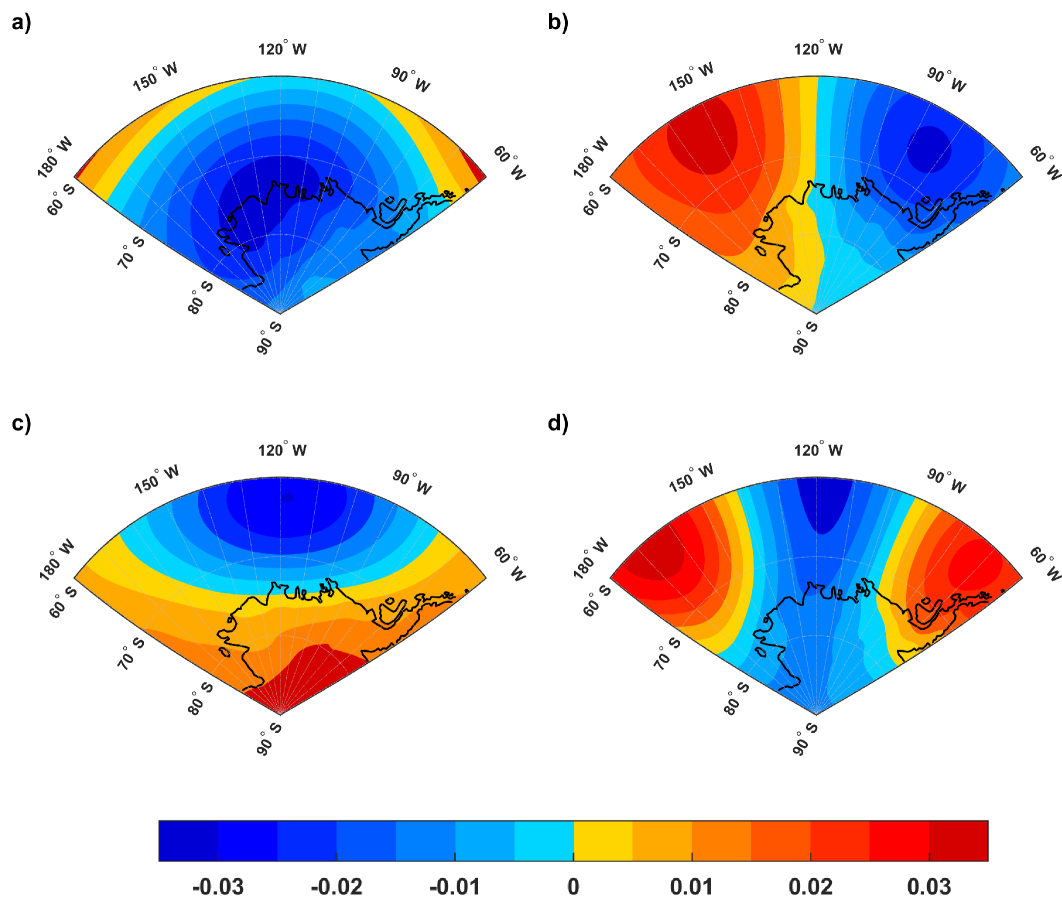


Figure 2. Spatial analysis of first four EOF modes (a,b,c and d) of daily geopotential height at 850 hPa over the region 60° S to 90° S and 180° W to 60° W.

171 Table S1). Given the strong correlation with precipitation over the rest of the domain,
 172 a similar frequency distribution and seasonal variability is expected over most of the WA
 173 domain. The rest of this section will focus on identifying the key drivers of EPEs at the two
 174 locations.

175 3.1 Dominant patterns of atmospheric variability over coastal WA

176 The dominant modes of near-surface atmospheric circulation over the study domain are
 177 identified from the EOF analysis of daily geopotential height anomalies at 850 hPa. The
 178 first dominant mode (EOF-1) which explains $\sim 48\%$ of the total variability is the Southern
 179 Annular Mode (SAM, Limpasuvan and Hartmann (1999); Thompson and Wallace (2000)).
 180 The spatial pattern is associated with an annular structure and a negative anomaly centred
 181 at 130° W (Figure-2a). The first PC time series shows a strong positive correlation (> 0.7)
 182 with SAM and it has a weak negative correlation with ASL- actual central pressure index
 183 (Supplementary Table S2).

184 The second EOF mode (EOF-2) (Figure-2b) explains $\sim 19\%$ variability. The spatial pat-
 185 tern is characterised by positive anomalies centred at 150° W (Amundsen Sea region in the
 186 western WA) and negative anomalies centred at 90° W (west of Antarctic Peninsula). This
 187 spatial pattern, consisting of pressure anomalies of opposite signs to the west of Antarctic
 188 Peninsula and over the Amundsen Sea region, is representative of the western branch of the
 189

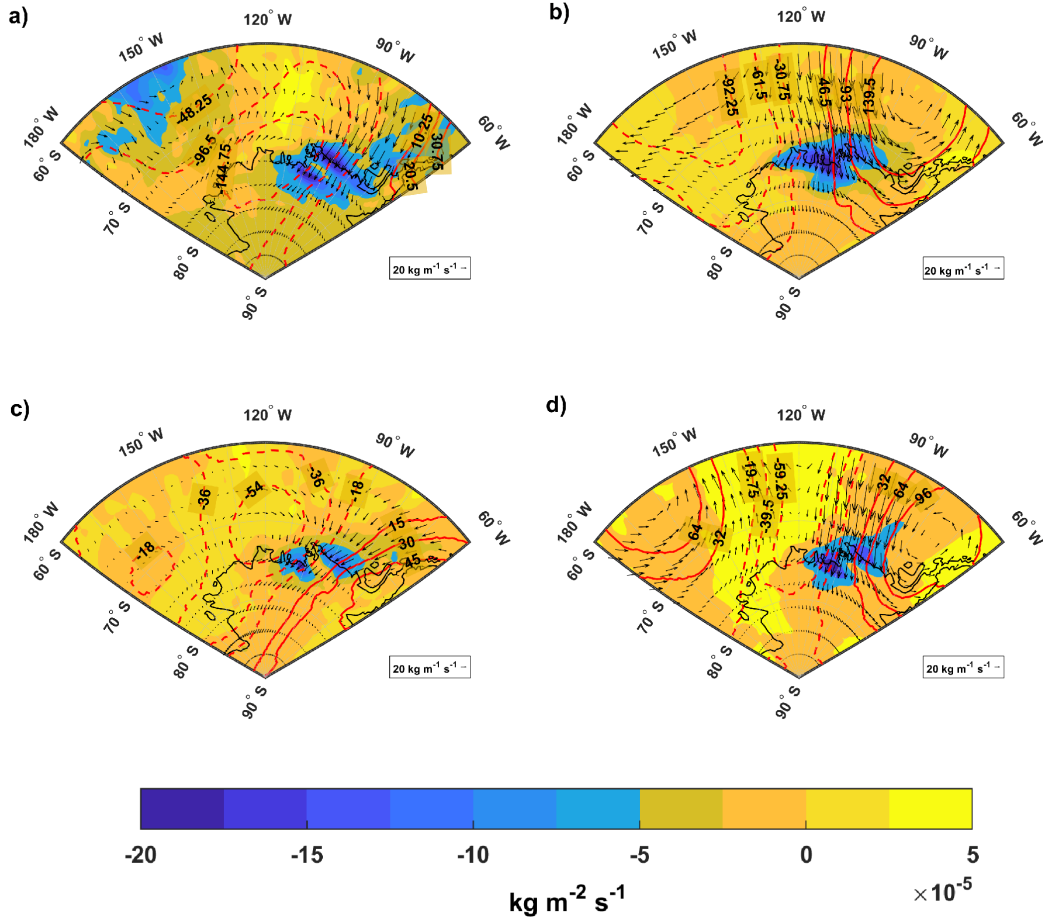


Figure 3. Composite anomalies of moisture divergence (shaded, in $\text{kg m}^{-2} \text{s}^{-1}$), moisture transport (vectors, in $\text{kg m}^{-1} \text{s}^{-1}$) and geopotential height at 850 hpa (positive and negative anomalies are represented by red solid lines and red dotted contours, respectively) during EPE days at EK, when only respective PC-1 (a), PC-2 (b), PC-3 (c) and PC-4 (d) modes are dominant.

190 PSA2 pattern. The change in polarity of this pattern (equivalent to a zonal shift in ASL)
 191 can be conveniently represented by the ASL lon index as presented in Deb et al. (2018).
 192 This is evident from a strong positive correlation (> 0.9) of the corresponding PC with
 193 ASL-lon index (Table S2).
 194

195 The spatial pattern of EOF-3 mode (Figure-2c), which accounts for $\sim 17.14\%$ of total
 196 variability, resembles the ENSO spatial pattern with positive (negative) anomalies over
 197 Amundsen Sea during El Niño (La Niña) events (Clem & Fogt, 2013; Deb et al., 2018).
 198 The modulation of this mode by eastern Pacific Ocean is further evident from a significant
 199 negative correlation (~ -0.5) of the PC time series with ENSO-ONI index (Table S2).
 200

201 The EOF-4 mode explains around 8.04% of the total variability, and this is a structure
 202 that may be conducive for more ‘atmospheric river’ activity consisting of an elongated neg-
 203 ative anomaly pattern extending from mid latitudes onto the continent (Figure-2d). The
 204 pattern, along with the blocking structures on either sides, shows close proximity to the
 205 observed atmospheric river pattern mentioned in Wille et al. (2019).
 206

3.2 Role of the main atmospheric modes in driving EPEs over coastal WA

A particular atmospheric mode is considered to play the dominant role during an EPE day if the corresponding PC on that day shows the largest value among the 4 major modes. Composites of 3 important variables (e.g., divergence of moisture flux, moisture transport and geopotential height anomalies at 850 hPa) are computed during EPE days at EK dominated by each individual mode (Figure-3). For example, Figure-3a shows the composite for EPE days dominated by the first EOF mode. A cyclonic geopotential height anomaly is noticed over coastal WA which is consistent with the spatial pattern of EOF-1 mode in Figure-2a. A strong meridional moisture transport towards the continent leads to intense moisture convergence (magnitude $> 5 \times 10^{-5} \text{ kgm}^{-2}\text{s}^{-1}$) along the eastern WA coastline (between 120°W and 60°W) and western Antarctic Peninsula (blue shading). This circulation anomaly explains the occurrence of EPEs at EK station during the days dominated by first mode of atmospheric variability over WA, i.e., the SAM.

Figure-3b shows that the EPE days at EK that are dominated by the second EOF mode show a dipole-like geopotential anomaly pattern with anti-cyclonic and cyclonic anomaly centres to the east (west) of $\sim 110^\circ\text{W}$. This pattern (which is clearly similar to spatial pattern of the second EOF mode) drives a strong meridional moisture transport towards the WA coast, with the strongest moisture convergence (magnitude $> 5 \times 10^{-5} \text{ kg/m/s}$) concentrated over the ASE ($140^\circ\text{W} - 90^\circ\text{W}$).

Atmospheric circulation pattern during EPE days (at EK) dominated by the third EOF mode is shown in Figure-3c. Similar to the spatial pattern of EOF-3 (as shown in Figure-2c), a cyclonic circulation anomaly is observed over the Amundsen Sea region accompanied by anomalous moisture transport towards the coastal WA leading to intense moisture convergence along the coastline. However, the area of the strongest moisture convergence (i.e., magnitude $> 5 \times 10^{-5} \text{ kgm}^{-2}\text{s}^{-1}$) is limited within the ASE (e.g., $100^\circ\text{W} - 80^\circ\text{W}$ longitude belt). Therefore, the cyclonic circulation anomaly associated with the third mode can bring large quantities of moisture towards the coastal stations over the ASE and cause EPEs.

EPE days at EK that are dominated by EOF-4 mode shows the most favourable pattern for producing atmospheric rivers (Figure-3d). This is further supported by composite of moisture transport anomalies during EPE days dominated by EOF-4 which shows a distinct band of moisture inflow from the mid-latitudes (Supplementary figure-S5b). This pattern is associated with strong moisture transport towards the coastal WA and leads to intense moisture convergence with particularly large values (magnitude $> 5 \times 10^{-5} \text{ kgm}^{-2}\text{s}^{-1}$) concentrated over the ASE ($110^\circ\text{W} - 80^\circ\text{W}$ longitude belt).

Similarly, the composite anomalies during EPE days at BP when dominated by 4 individual EOF modes (Supplementary figure-S3) are broadly similar to that in the case of EK (i.e., Figure-3), particularly for EOF-2 and EOF-4. However, the anomaly centres corresponding to EOF-1 and EOF-3 are slightly shifted to the west when compared to Figure-3. Also, the spatial extent and magnitude of moisture convergence is less when compared to that of EK (Figure-3). Overall, the magnitude of precipitation associated with EOF-2 mode (ASL-lon) and EOF-4 mode (suspected atmospheric rivers) is larger by at least 2 mm/day over ASE compared to other modes (Supplementary figure-S4).

3.3 Relative seasonal contribution of different atmospheric modes

Figure-4a and 4b indicates the seasonal contribution of EOFs to EPEs at the two coastal locations over WA while the ‘total’ contribution of the EOF modes is shown in Figure-4c and d. The second EOF mode or the ASL-lon zonal pattern (i.e., the coupling of ASL with a blocking high over the Antarctic Peninsula) was found to be the leading driver of EPEs over coastal WA with a total contribution of 40.28% (49.23 %) at EK (BP) (Figure-4c and 4d). This pattern was previously reported to be the main driver of high snowfall events over

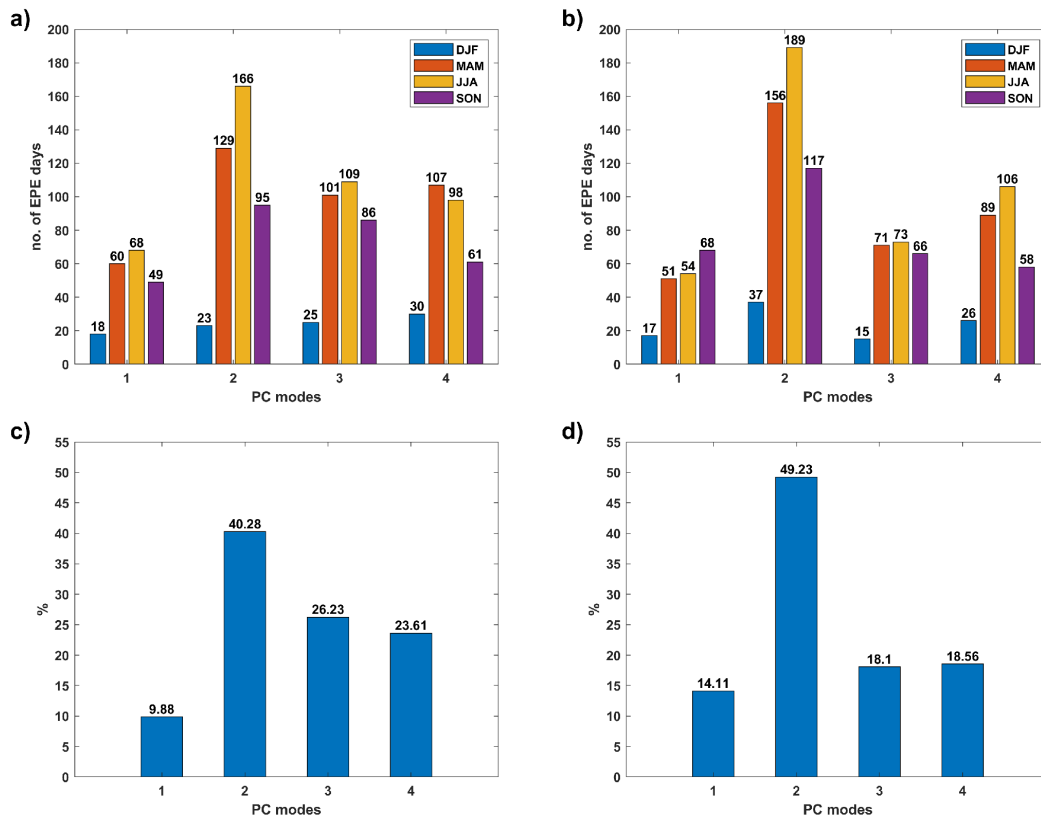


Figure 4. Seasonal distribution of EPE days occurring with respective PCs at (a) EK and (b) BP. Total contribution of dominant PCs to EPEs of (c) EK and (d) BP during the period 1979-2016.

Thwaites Glacier region of WA (MacLennan & Lenaerts, 2021). The pattern is particularly important for EPEs during MAM, JJA and SON seasons (Figure-4a and 4b). This is followed by EOF-3 (representative of ENSO influence over WA) and EOF-4 (suspected to be linked to the intrusion of atmospheric rivers) modes with percentage contributions of 26.23 and 23.61, respectively, to EPE days at EK (Figure-4c). Their respective contribution is 18.1 % and 18.56 % at BP (Figure-4d). On average, EOF-4 is slightly more dominant than EOF-3 during DJF, MAM and JJA seasons while EOF-3 is more dominant in SON (Figure-4a and 4b). In contrast, the first EOF mode associated with SAM showed the least percentage contribution to EPE days in all four seasons. The total contribution of EOF-1 to EPE days is 9.88 % and 14.11 % at EK and BP, respectively.

4 Discussion and Conclusions

Despite several attempts to understand the seasonal and inter annual changes in mass balance and precipitation over WA, only a few studies have attempted to understand the short lived extreme precipitation events and their atmospheric drivers. Most of annual precipitation over the coastal WA comes from EPEs (Turner et al., 2019). For example, we find that at two coastal stations over the ASE of WA (EK and BP), EPEs at EK and BP contributes around 41% of the total precipitation, with the maximum contribution from EPEs noted in JJA followed by MAM, SON and DJF seasons. As EK and BP are representative of the precipitation over the coastal WA, and also over inland areas (as evident from the significantly high correlation in Figure-1e and 1f), precipitation from these two stations are used to understand the frequency distribution and drivers of EPEs over coastal WA, and particularly the ASE.

The ‘ASL-lon’ pattern or the zonally coupled structure consisting of ASL and a blocking high over the Antarctic Peninsula was found to be the leading driver of EPEs over the ASE. Total contribution from ‘ASL-lon’ pattern to EPEs at the coastal stations over the ASE ($\sim 40 - 49\%$) is significantly higher than the total contribution from PSA-1 pattern ($\sim 18 - 26\%$) and the atmospheric river pattern ($\sim 18 - 24\%$) (Figure-4c and 4d). The ‘ASL-lon’ pattern was previously shown to be responsible for high snowfall events over Thwaites Glacier region of WA in a previous study (MacLennan & Lenaerts, 2021). ASL-lon pattern shows the maximum (minimum) contribution to EPEs in JJA (DJF). This seasonality in the contribution of ASL-lon is due to the well-defined annual cycle in the zonal location of ASL with a clear westward movement towards the Ross Sea in JJA which drives strong northerly wind into the ASE (J. S. Hosking et al., 2013; M. N. Raphael et al., 2016).

El Niño years associated with a large positive geopotential height anomaly centre off the coast of WA which drives anomalous warm and moist air advection into the WA ice sheet (Welhouse et al., 2016; Deb et al., 2018). The local circulation changes during El Niño years are associated with an increased likelihood of extreme surface temperature (Deb et al., 2018), and an increase in precipitation over the ASE (Paolo et al., 2018; Zhang et al., 2021). The ENSO signal over WA is captured by EOF-3 mode in our study, and explains more than 25% of the EPEs over coastal WA.

In our analysis, EOF-4 mode (suspected AR pattern) explains only 8% of the total variability, but it is associated with the most intense moisture convergence among all the modes (Figure-4). Despite their extreme rarity, atmospheric rivers have been linked to a number of heavy precipitation events across Antarctica (Gorodetskaya et al., 2014; Wille et al., 2019; Adusumilli et al., 2021). Our analysis shows that during the simulation period of 1979-2016, PC-4 mode is associated with approximately 18-23% of the extreme snowfall days over ASE (Figure-4c and 4d). However, their contribution in terms of the actual amount of snowfall will be much higher as the EPEs during PC-4 mode are much more intense (Supplementary figure-S4) due to the high moisture convergence.

313 As a large fraction of the precipitation over coastal WA comes from EPEs, the future
 314 mass balance changes over WA will be highly sensitive to the future changes in the atmo-
 315 spheric drivers of EPEs identified in this study. A westward (and poleward) shift of ASL
 316 (J. S. Hosking et al., 2016; Brown et al., 2020) along with a likely increase in the frequency
 317 of atmospheric rivers land falling on Antarctica by the end of the 21st century (Espinoza et
 318 al., 2018; Payne et al., 2021) are expected to make a positive contribution to future mass
 319 balance changes over WA. However, projected change in ENSO, and hence the associated
 320 teleconnection, remain highly uncertain. Therefore, it is essential that the dynamics of these
 321 drivers and their interaction with the WA coastline are well-understood in order to constrain
 322 the future mass balance changes over ASE and coastal WA.

323 5 Open Research

324 Data availability statement

325 All the datasets for this research are openly available online.
 326 RACMO version 3p2 limited area atmospheric model precipitation data used in this study is
 327 available online through British Antarctic Survey repository : [https://doi.org/10.5285/
 328 bbf12a6f-7d97-4951-9bd1-e4224e2abac9](https://doi.org/10.5285/bbf12a6f-7d97-4951-9bd1-e4224e2abac9)
 329 ERA-Interim data is available at European Centre for Medium-Range Weather Forecasts
 330 (ECMWF) : <https://apps.ecmwf.int/datasets/>
 331 ENSO Oceanic Niño Index (ONI) is obtainable from National Weather Service, Climate Pre-
 332 diction Center : [https://origin.cpc.ncep.noaa.gov/products/analysis_monitoring/
 333 ensostuff/ONI_v5.php](https://origin.cpc.ncep.noaa.gov/products/analysis_monitoring/ensostuff/ONI_v5.php)
 334 Marshall Southern Annular Mode (SAM) index available at : [http://www.nerc-bas.ac
 335 .uk/icd/gjma/sam.html](http://www.nerc-bas.ac.uk/icd/gjma/sam.html)
 336 Amundsen Sea Low (ASL) index available at : http://scotthosking.com/asl_index

337 Acknowledgments

338 Both the authors were funded by the Indian Institute of Technology Kharagpur and the
 339 Ministry of Education, Govt. of India. We also acknowledge the support of the National
 340 Centre for Polar and Ocean Research, Goa (project: NCPOR/2019/PACER-POP/AS-02).
 341

342 References

- 343 Adusumilli, S., A Fish, M., Fricker, H. A., & Medley, B. (2021). Atmospheric river precipi-
 344 tation contributed to rapid increases in surface height of the west antarctic ice sheet
 345 in 2019. *Geophysical Research Letters*, *48*(5), e2020GL091076.
- 346 Banta, J. R., McConnell, J. R., Frey, M. M., Bales, R. C., & Taylor, K. (2008). Spatial and
 347 temporal variability in snow accumulation at the west antarctic ice sheet divide over
 348 recent centuries. *Journal of Geophysical Research: Atmospheres*, *113*(D23).
- 349 Brown, J. R., Brierley, C. M., An, S.-I., Guarino, M.-V., Stevenson, S., Williams, C. J., . . .
 350 others (2020). Comparison of past and future simulations of enso in cmip5/pmip3
 351 and cmip6/pmip4 models. *Climate of the Past*, *16*(5), 1777–1805.
- 352 Clem, K. R., & Fogt, R. L. (2013). Varying roles of enso and sam on the antarctic peninsula
 353 climate in austral spring. *Journal of Geophysical Research: Atmospheres*, *118*(20),
 354 11–481.
- 355 Clem, K. R., & Fogt, R. L. (2015). South pacific circulation changes and their connection
 356 to the tropics and regional antarctic warming in austral spring, 1979–2012. *Journal
 357 of Geophysical Research: Atmospheres*, *120*(7), 2773–2792.
- 358 Deb, P., Orr, A., Bromwich, D. H., Nicolas, J. P., Turner, J., & Hosking, J. S. (2018).
 359 Summer drivers of atmospheric variability affecting ice shelf thinning in the amundsen
 360 sea embayment, west antarctica. *Geophysical Research Letters*, *45*(9), 4124–4133.

- 361 Deb, P., Orr, A., Hosking, J. S., Phillips, T., Turner, J., Bannister, D., ... Colwell, S.
 362 (2016). An assessment of the polar weather research and forecasting (wrf) model
 363 representation of near-surface meteorological variables over west antarctica. *Journal*
 364 *of Geophysical Research: Atmospheres*, *121*(4), 1532–1548.
- 365 Dee, D. P., Uppala, S. M., Simmons, A. J., Berrisford, P., Poli, P., Kobayashi, S., ...
 366 others (2011). The era-interim reanalysis: Configuration and performance of the data
 367 assimilation system. *Quarterly Journal of the royal meteorological society*, *137*(656),
 368 553–597.
- 369 Déry, S. J., & Yau, M. (1999). A bulk blowing snow model. *Boundary-Layer Meteorology*,
 370 *93*(2), 237–251.
- 371 Espinoza, V., Waliser, D. E., Guan, B., Lavers, D. A., & Ralph, F. M. (2018). Global anal-
 372 ysis of climate change projection effects on atmospheric rivers. *Geophysical Research*
 373 *Letters*, *45*(9), 4299–4308.
- 374 Ettema, J., Van den Broeke, M., Van Meijgaard, E., Van de Berg, W., Box, J., & Steffen, K.
 375 (2010). Climate of the greenland ice sheet using a high-resolution climate model—part
 376 1: Evaluation. *The Cryosphere*, *4*(4), 511–527.
- 377 Ghil, M., & Mo, K. (1991). Intraseasonal oscillations in the global atmosphere. part ii:
 378 Southern hemisphere. *Journal of Atmospheric Sciences*, *48*(5), 780–790.
- 379 Giorgi, F., Shields Brodeur, C., & Bates, G. T. (1994). Regional climate change scenarios
 380 over the united states produced with a nested regional climate model. *Journal of*
 381 *Climate*, *7*(3), 375–399.
- 382 Gorodetskaya, I. V., Tsukernik, M., Claes, K., Ralph, M. F., Neff, W. D., & Van Lipzig,
 383 N. P. (2014). The role of atmospheric rivers in anomalous snow accumulation in east
 384 antarctica. *Geophysical Research Letters*, *41*(17), 6199–6206.
- 385 Hosking, J. S., Orr, A., Bracegirdle, T. J., & Turner, J. (2016). Future circulation changes
 386 off west antarctica: Sensitivity of the amundsen sea low to projected anthropogenic
 387 forcing. *Geophysical Research Letters*, *43*(1), 367–376.
- 388 Hosking, J. S., Orr, A., Marshall, G. J., Turner, J., & Phillips, T. (2013). The influence
 389 of the amundsen–bellingshausen seas low on the climate of west antarctica and its
 390 representation in coupled climate model simulations. *Journal of Climate*, *26*(17),
 391 6633–6648.
- 392 Hosking, S. (2020). *The climate data guide: Amundsen sea low indices*, edited by: National
 393 center for atmospheric research staff. Retrieved from [https://climatedataguide](https://climatedataguide.ucar.edu/climate-data/amundsen-sea-low-indices)
 394 [.ucar.edu/climate-data/amundsen-sea-low-indices](https://climatedataguide.ucar.edu/climate-data/amundsen-sea-low-indices)
- 395 Irving, D., & Simmonds, I. (2015). A novel approach to diagnosing southern hemisphere
 396 planetary wave activity and its influence on regional climate variability. *Journal of*
 397 *Climate*, *28*(23), 9041–9057.
- 398 Kidson, J. W. (1988). Interannual variations in the southern hemisphere circulation. *Journal*
 399 *of Climate*, *1*(12), 1177–1198.
- 400 Kuipers Munneke, P., Van den Broeke, M., Lenaerts, J., Flanner, M., Gardner, A., & Van de
 401 Berg, W. (2011). A new albedo parameterization for use in climate models over the
 402 antarctic ice sheet. *Journal of Geophysical Research: Atmospheres*, *116*(D5).
- 403 Lau, K., Sheu, P., & Kang, I.-S. (1994). Multiscale low-frequency circulation modes in the
 404 global atmosphere. *Journal of the Atmospheric Sciences*, *51*(9), 1169–1193.
- 405 Lenaerts, J., Van den Broeke, M., Déry, S., König-Langlo, G., Ettema, J., & Munneke, P. K.
 406 (2010). Modelling snowdrift sublimation on an antarctic ice shelf. *The Cryosphere*,
 407 *4*(2), 179–190.
- 408 Lenaerts, J. T., van Meijgaard, E., van den Broeke, M. R., Ligtenberg, S. R., Horwath, M., &
 409 Isaksson, E. (2013). Recent snowfall anomalies in droning maud land, east antarctica,
 410 in a historical and future climate perspective. *Geophysical Research Letters*, *40*(11),
 411 2684–2688.
- 412 Limpasuvan, V., & Hartmann, D. L. (1999). Eddies and the annular modes of climate
 413 variability. *Geophysical Research Letters*, *26*(20), 3133–3136.
- 414 MacLennan, M. L., & Lenaerts, J. T. (2021). Large-scale atmospheric drivers of snowfall over
 415 thwaites glacier, antarctica. *Geophysical Research Letters*, *48*(17), e2021GL093644.

- 416 Marshall, G. (2018). *The climate data guide: Marshall southern annular mode (sam) index*
 417 *(station-based)*, edited by: National center for atmospheric research staff.
- 418 Marshall, G. J., Thompson, D. W., & van den Broeke, M. R. (2017). The signature
 419 of southern hemisphere atmospheric circulation patterns in antarctic precipitation.
 420 *Geophysical Research Letters*, *44*(22), 11–580.
- 421 Mayewski, P. A., Meredith, M., Summerhayes, C., Turner, J., Worby, A., Barrett, P., ...
 422 others (2009). State of the antarctic and southern ocean climate system. *Reviews of*
 423 *Geophysics*, *47*(1).
- 424 Mo, K. C., & Paegle, J. N. (2001). The pacific–south american modes and their downstream
 425 effects. *International Journal of Climatology: A Journal of the Royal Meteorological*
 426 *Society*, *21*(10), 1211–1229.
- 427 Noone, D., & Simmonds, I. (1998). Implications for the interpretation of ice-core isotope
 428 data from analysis of modelled antarctic precipitation. *Annals of Glaciology*, *27*,
 429 398–402.
- 430 Orr, A., Phillips, T., Webster, S., Elvidge, A., Weeks, M., Hosking, S., & Turner, J. (2014).
 431 Met office unified model high-resolution simulations of a strong wind event in antarc-
 432 tica. *Quarterly Journal of the Royal Meteorological Society*, *140*(684), 2287–2297.
- 433 Paolo, F., Padman, L., Fricker, H., Adusumilli, S., Howard, S., & Siegfried, M. (2018).
 434 Response of pacific-sector antarctic ice shelves to the el niño/southern oscillation.
 435 *Nature geoscience*, *11*(2), 121–126.
- 436 Payne, A. J., Nowicki, S., Abe-Ouchi, A., Agosta, C., Alexander, P., Albrecht, T., ... others
 437 (2021). Future sea level change under coupled model intercomparison project phase
 438 5 and phase 6 scenarios from the greenland and antarctic ice sheets. *Geophysical*
 439 *Research Letters*, *48*(16), e2020GL091741.
- 440 Pritchard, H., Ligtenberg, S. R., Fricker, H. A., Vaughan, D. G., van den Broeke, M. R.,
 441 & Padman, L. (2012). Antarctic ice-sheet loss driven by basal melting of ice shelves.
 442 *Nature*, *484*(7395), 502–505.
- 443 Pritchard, H. D., Arthern, R. J., Vaughan, D. G., & Edwards, L. A. (2009). Extensive
 444 dynamic thinning on the margins of the greenland and antarctic ice sheets. *Nature*,
 445 *461*(7266), 971–975.
- 446 Raphael, M. (2004). A zonal wave 3 index for the southern hemisphere. *Geophysical*
 447 *Research Letters*, *31*(23).
- 448 Raphael, M. N., Marshall, G., Turner, J., Fogt, R., Schneider, D., Dixon, D., ... Hobbs,
 449 W. R. (2016). The amundsen sea low: variability, change, and impact on antarctic
 450 climate. *Bulletin of the American Meteorological Society*, *97*(1), 111–121.
- 451 Rignot, E., Bamber, J. L., Van Den Broeke, M. R., Davis, C., Li, Y., Van De Berg, W. J.,
 452 & Van Meijgaard, E. (2008). Recent antarctic ice mass loss from radar interferometry
 453 and regional climate modelling. *Nature geoscience*, *1*(2), 106–110.
- 454 Rignot, E., Mouginot, J., Scheuchl, B., Van Den Broeke, M., Van Wesseem, M. J., &
 455 Morlighem, M. (2019). Four decades of antarctic ice sheet mass balance from 1979–
 456 2017. *Proceedings of the National Academy of Sciences*, *116*(4), 1095–1103.
- 457 Sodemann, H., & Stohl, A. (2009). Asymmetries in the moisture origin of antarctic precip-
 458 itation. *Geophysical research letters*, *36*(22).
- 459 Summerhayes, C., Ainley, D., Barrett, P., Bindschadler, R., Clarke, A., Convey, P., ...
 460 others (2009). The antarctic environment in the global system. *Antarctic climate*
 461 *change and the environment. Scientific Committee on Antarctic Research, Cambridge*,
 462 1–32.
- 463 Thompson, D. W., & Wallace, J. M. (2000). Annular modes in the extratropical circulation.
 464 part i: Month-to-month variability. *Journal of climate*, *13*(5), 1000–1016.
- 465 Turner, J., Bindschadler, R., Convey, P., Di Prisco, G., Fahrbach, E., Gutt, J., ... Sum-
 466 merhayes, C. (2009). *Antarctic climate change and the environment*.
- 467 Turner, J., Phillips, T., Thamban, M., Rahaman, W., Marshall, G. J., Wille, J. D., ...
 468 others (2019). The dominant role of extreme precipitation events in antarctic snowfall
 469 variability. *Geophysical Research Letters*, *46*(6), 3502–3511.

- 470 Undén, P., Rontu, L., Järvinen, H., Lynch, P., Calvo, J., Cats, G., ... others (2002).
471 Hirlam-5 scientific documentation.
- 472 Van Wessem, J., Reijmer, C., Morlighem, M., Mougnot, J., Rignot, E., Medley, B., ...
473 others (2014). Improved representation of east antarctic surface mass balance in a
474 regional atmospheric climate model. *Journal of Glaciology*, 60(222), 761–770.
- 475 Vaughan, D. G., Marshall, G. J., Connolley, W. M., King, J. C., & Mulvaney, R. (2001).
476 Devil in the detail. *Science*, 293(5536), 1777–1779.
- 477 Welhouse, L. J., Lazzara, M. A., Keller, L. M., Tripoli, G. J., & Hitchman, M. H. (2016).
478 Composite analysis of the effects of enso events on antarctica. *Journal of Climate*,
479 29(5), 1797–1808.
- 480 Wille, J. D., Favier, V., Dufour, A., Gorodetskaya, I. V., Turner, J., Agosta, C., & Co-
481 dron, F. (2019). West antarctic surface melt triggered by atmospheric rivers. *Nature*
482 *Geoscience*, 12(11), 911–916.
- 483 Zhang, B., Yao, Y., Liu, L., & Yang, Y. (2021). Interannual ice mass variations over the
484 antarctic ice sheet from 2003 to 2017 were linked to el niño-southern oscillation. *Earth*
485 *and Planetary Science Letters*, 560, 116796.
- 486 Zhu, Y., & Newell, R. E. (1998). A proposed algorithm for moisture fluxes from atmospheric
487 rivers. *Monthly weather review*, 126(3), 725–735.
- 488 Zwally, H. J., Robbins, J. W., & Luthcke, S. B. (2017). Mass balance of east antarctic ice
489 sheet: Reconciling icesat altimetry with grace gravimetry and long-term ice history.
490 In *Agu fall meeting abstracts* (Vol. 2017, pp. C23D–08).